Near-resonance Light Scattering from a High-density, Ultracold Atomic ^{87}Rb Gas

S. Balik, A.L. Win and M.D. Havey
*Department of Physics, Old Dominion University, Norfolk, VA 23529**

I.M. Sokolov and D.V. Kupriyanov
Department of Theoretical Physics, State Polytechnic University, 195251, St.-Petersburg, Russia
(Dated: September 8, 2009)

We report experimental investigation of hyperfine optical pumping and near resonance light scattering from a high-density and ultracold atomic ^{87}Rb gas. The atomic sample, having a peak density $\sim 5 \cdot 10^{13}$ atoms/cm^3, temperature ~ 65 μK and initially prepared in the F = 1 lower energy ^{87}Rb hyperfine component, is optically pumped to the higher energy F = 2 hyperfine level. Measurements are made of the transient hyperfine pumping process and of the time evolution of scattering of near resonance probe radiation on the $F = 2 \rightarrow F' = 3$ transition. Features of the density, detuning, and probe laser intensity dependence of the signals are attributed to the high peak density and consequent large optical depth of the samples.

PACS numbers: 42.25.Dd, 42.50.Nn, 42.50.-P, 72.15.Rn, 37.10.Gh

I. INTRODUCTION

Development of techniques to cool and trap atomic gases [1, 2] has revolutionized many traditional atomic physics research areas and, at the same time, has stimulated new connections and types of interdisciplinary specialization. Even if one does not consider vital research involving quantum degenerate gases [3, 4], areas such as quantum information [5, 6], quantum optics [7, 8, 9, 10], precision measurements [11, 12, 13], plasma physics [14, 15], and molecular spectroscopy [16, 17] have been transformed by the combination of ultracold experimental facility and theoretical understanding of the physical processes. Among the important characteristics of utilized atomic gases are the gas temperature, density, and spin polarization. For example, storage of individual photon wave packets in ultracold gases combines quantum optical techniques of coherent dark state formation and electromagnetically induced transparency to address a critical area of quantum information processing [18, 19]. The lifetime of the atomic spin wave, which determines the storage time of the photonic information in the form of a dark state polariton, depends on the gas temperature, collision rates, and local magnetic environment. In another research area, photoassociative formation of ultracold diatomic molecules depends quadratically on the density of the parent ultracold atomic gas. Likewise, by initiating formation of an ultracold plasma in a high density atomic gas, one can attain strong coupling with sufficient ionization of the gas.

Over the past decade, a number of research groups [20, 21, 22, 23, 24, 25, 26] have concentrated on near-resonance light scattering in ultracold atomic gases. A particular interest has been in coherent multiple scattering of light when the influence of atomic motion is of minimal importance. Then the natural length scale for the photon multiple scattering is the optical mean-free-path, given by $l = 1/\rho\sigma$, where ρ is the atomic density and σ the cross-section for atomic light scattering in a weak field. For light of wave vector magnitude $k = 2\pi/\lambda$, a useful dimensionless parameter is kl [27]. When kl $>>$ 1, the so called weak localization regime [22], light scattering can be thought of as a sequence of scattering and propagation events [23]. In this regime, an observable that survives configuration averaging is the coherent backscattering cone, which is a few milliradian-width feature that displays an enhancement of as much as a factor of two over the incoherent albedo for back scattered light [28, 29, 30]. In ultracold atomic gases, the angular shape and peak enhancement of this spectral feature has been studied for a wide range of conditions, including spectral detuning from resonance, light polarization, probe light intensity [31], sample size and optical density, and external magnetic field [32, 33, 34, 35, 36, 37, 38, 39, 40]. Observation of the coherent backscattering cone established that multiple light scattering, even for resonance radiation, is a coherent process. When the atomic density is significantly increased, so that the parameter kl $\sim$ 1 (the so-called Ioffe-Regel condition [27]), there are a number of atoms within a volume $1/k^3$, and light scattering [41] becomes a cooperative process [22, 42, 43]. In this regime, it is expected that a number of fascinating quantum optical processes, including Anderson localization of light [44, 45, 46, 47, 48], and random atom-based lasing [49, 50, 51, 52, 53], may emerge. It is these processes, and the conditions under which they might be experimentally studied, that are the main motivation for the current research program.

Before we present our experimental procedures, results and associated discussions, let us make a few remarks concerning the definitions and parametrization we follow throughout the paper. Most of the reported experimental data relate to a relatively high density atomic system. For the considered densities, which are at the

*Electronic address: mhavey@odu.edu

level of more than one atom per cubic wavelength, it appears that the atomic system should have properties approaching those of a bulk medium. From a classical point of view the relevant theoretical description then would require us to introduce a mesoscopically smoothed dielectric constant ϵ and treat the light scattering process through secondary or multiply scattered waves created by fluctuations in ϵ. If the fluctuation scale of ϵ were much smaller than its mean value then the light transport through the sample would be fairly approximated by a perturbation theory analysis of the macroscopic Maxwell equations, [54]. Apparently, such an approximation would be excellent in a weak disorder regime [23] at low densities when $\epsilon \sim 1$. For the peak values of the atom densities attained in our experiments the variation of the dielectric constant is expected to be still quite close to the vacuum level [42]. This justifies the parametrization of our data in the standard terms normally valid for a dilute configuration, such as the vacuum scattering cross section, the mean free path for light scattering, and the optical depth. These quantities seem to us to be convenient for qualitative description and discussion. However at certain points of our analysis we will pay attention to the evidence of the effects of macroscopic electrodynamics, see Section III. C. We would also like to point out that at a further increase in density by only several times, the situation dramatically changes and turns toward a highly disorder regime. As expected, in this case the average dielectric constant would have the same order of magnitude as its fluctuations, and the system would demonstrate some specific spectral properties of a collectivized quantum system [42, 43]. These properties have a signature of strong correlation with each particular configuration of atomic scatterers, and can be linked with the Anderson-type localization conditions for electromagnetic waves. Part of the single dipole excitations associated with the collective resolvent poles would have a long-lived sub-radiant nature.

In the present paper, we describe our experimental approach to obtaining atomic conditions, and particularly atomic densities, in the regime where $\mathrm{k}l \sim 1$. We also describe the method we use to prepare the atomic sample so that large orders of multiple scattering may be obtained, along with the associated experimental observations and their interpretation. This is followed by presentation and discussion of experimental results of density, detuning, and light intensity dependence of light scattering on the nearly-closed $\mathrm{F} = 2 \rightarrow \mathrm{F}' = 3$ hyperfine component of the ^{87}Rb D2 transition.

II. EXPERIMENTAL APPROACH

A schematic of the experimental apparatus is shown in Fig. 1, and the main optical excitation transitions used in the present experiments are shown in Fig. 2. In Fig. 1, the main focus of the instrumentation is an optical dipole trap formed in the focal region of a carbon-dioxide (CO_2) laser. A 40 MHz acousto optical modulator (AOM) is used to switch and to direct approximately 50 W of the 100 W CO_2 laser output to the trapping region. The trapping beam is focussed to a radial spot size of ~ 55 μm, and associated Rayleigh range of $z_R \sim 750$ μm. Because the operating trap wavelength of 10.6 μm is far longer than those of the Rb resonance transitions, the dipole force is closely proportional to the static dipole polarizability of atomic Rb; the trap is then referred to as a quasistatic electric dipole trap (QUEST) [2]. The trap depth is approximately 650 μK, and has associated measured trap angular frequencies $\omega_z = 2\pi \cdot 50$ rad/s and $\omega_r = 2\pi \cdot 1300$ rad/s. As described in detail elsewhere [55], the QUEST is loaded with atoms that have been collected from a surrounding thermal Rb vapor and cooled in an overlapping magneto optical trap (MOT). The QUEST atoms are initially loaded into the lower en-

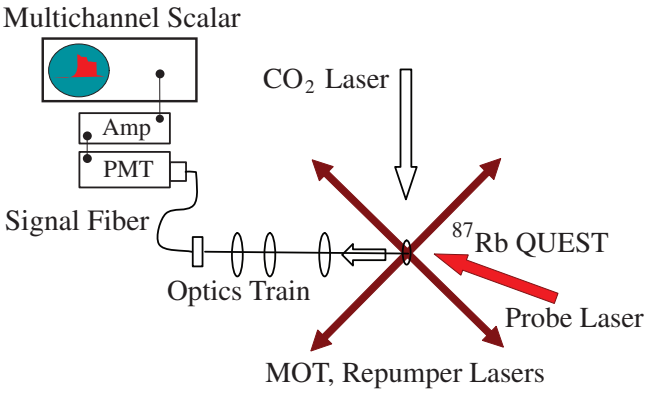

FIG. 1: Schematic drawing of the experimental apparatus. In the figure QUEST stands for quasi electrostatic trap, PMT refers to a photomultiplier tube, and CCD represents a charge coupled device camera. MOT refers to a magneto-optical trap, while CO_2 laser indicates a carbon-dioxide laser. Drawing not to scale.

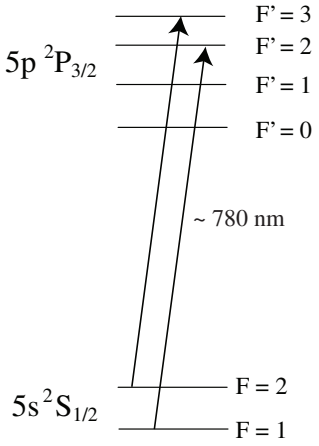

FIG. 2: Schematic energy level diagram for ^{87}Rb showing the optical transitions important for the experiments reported in this paper. Not to scale.

ergy F = 1 hyperfine component of the Rb ground level. Following QUEST loading, the MOT lasers and magnetic fields are shut off, and the atoms in the dipole trap collisionally thermalize to a temperature of approximately 65 μK. After this natural thermalization process, approximately 15 % of the atoms originally in the MOT have been transferred to the QUEST. Measurements of the QUEST characteristics, after the hold period, by absorption imaging, parametric resonance, and the measured number of atoms transferred show a sample with peak density about $5 \cdot 10^{13}$ $atoms/cm^3$ and a temperature of $T_o = 65$ μK. The 1/e lifetime of the confined atoms is greater than 5 s, limited by background gas collisions.

The primary goal of the experiments is to study light scattering on the nearly closed $F = 2 \rightarrow F' = 3$ hyperfine transition associated with the D2 resonance line. However, the atoms are initially loaded into the QUEST in the F = 1 lower energy hyperfine component, and must be optically pumped into the higher energy F = 2 level. This is accomplished by the MOT repumping laser beams, tuned resonantly to the $F = 1 \rightarrow F' = 2$ transition as indicated in Fig. 2. The repumper laser is an external cavity diode laser, and is locked to an ^{87}Rb saturated absorption feature associated with the $F = 1 \rightarrow F' = 2$ hyperfine transition. The laser bandwidth is approximately 0.5 MHz. The repumper delivers a beam of maximum intensity ~ 4 mW/cm^2 and is directed along the same optical paths as the trapping laser beams. Repumper switching is controlled with an acousto optical modulator. There are three counter propagating pairs of such beams directed towards the sample along three orthogonal directions. The repumper intensity of ~ 4 mW/cm^2 corresponds to an on-resonance saturation parameter larger than unity. With reference to Fig. 1, the light scattered out of the repumper beams by the atom sample is collected at an angle of 45 degrees from the horizontal pair of repumper beams and at 90 degrees from the vertical beam pair (not shown). Approximately 1 % of the resulting scattered light is collected with a field lens and launched into a multimode fiber which, in turn, transports the light to an infrared sensitive and refrigerated photomultiplier tube (PMT) operating in a single photon counting mode. The photon counting pulses are amplified with a fast amplifier and then binned in a multichannel scalar (MCS) with a time resolution of 5 ns. Depending on the counting rate, a data record of several thousand experimental realizations is necessary to obtain sufficient counting statistics.

In the main experimental protocol, a probe beam tuned in the spectral vicinity of the $F = 2 \rightarrow F' = 3$ nearly closed transition is directed towards the sample, and the resulting scattered light signals collected by the same optical arrangement described above. The probe laser is of the same design as the repumper laser, has a bandwidth ~ 3 MHz, and is switched and directed by an acousto optical modulator towards the sample. Because of constraints on the vacuum chamber geometry, the linearly polarized probe beam is directed (see Fig. 1) at an angle of approximately 30 degrees away from the fluorescence collection direction. The probe beam is also directed downwards at an angle of 30 degrees. The collection and electronic accumulation of scattered light signals is the same as with the repumper signals. We should point out that the two protocols described above are applied separately or together, and with varied relative time separation, depending on the specific experiments of interest. These different approaches are described individually, and as appropriate for each data set, in the following sections.

Peak b_t	n_o (atoms/cm^3)	r_o (μm)	z_o (μm)
165	5.0×10^{13}	9.8	248
117	2.5×10^{13}	13.8	248
82	1.2×10^{13}	19.5	248
53	5.1×10^{12}	30.4	249
16	5.2×10^{11}	92.3	264
5	5.9×10^{10}	240	345

TABLE I: QUEST parameters relating the peak transverse optical depth on the $F = 1 \rightarrow F' = 2$ transition to the peak sample density and the Gaussian radii of the atomic cloud.

To close this section, we point out that in some of the experiments reported here the atomic density was varied over a wide range. This was accomplished by allowing for a period of ballistic expansion of the cloud after the QUEST was turned off. The atomic sample temperature is known, so this procedure allows the peak density or the peak optical depth to be determined. As the sample is well approximated by a two-axis Gaussian atom distribution [56], the two Gaussian radii and the peak atom density (or the total number of atoms in the sample), are sufficient to determine the two peak optical depths characterizing the sample. We summarize in Table 1 the peak transverse optical depth b_t the peak atom density at the center of the sample n_o, the transverse Gaussian radius r_o, and the longitudinal Gaussian radius z_o. The optical depth refers here to that of the nearly closed $F = 2 \rightarrow F' = 3$ hyperfine transition, and is obtained by using a resonance scattering cross section of $1.36 \times 10^{-9} cm^2$. The optical depth dependence may readily be rescaled to other $F \rightarrow F'$ transitions [56].

III. RESULTS

A. Hyperfine Optical Pumping

In this section, we focus on the hyperfine optical pumping process, by which the ^{87}Rb atoms in the QUEST are brought from the F = 1 to the F = 2 ground hyperfine component. Fluorescence signals taken over a three order of magnitude range of sample density are shown in Fig. 3. These densities, as indicated in the figure legend, represent the peak density in the central region of the atomic sample. As described in an earlier section of the paper, the sample density is reduced from its maximum value

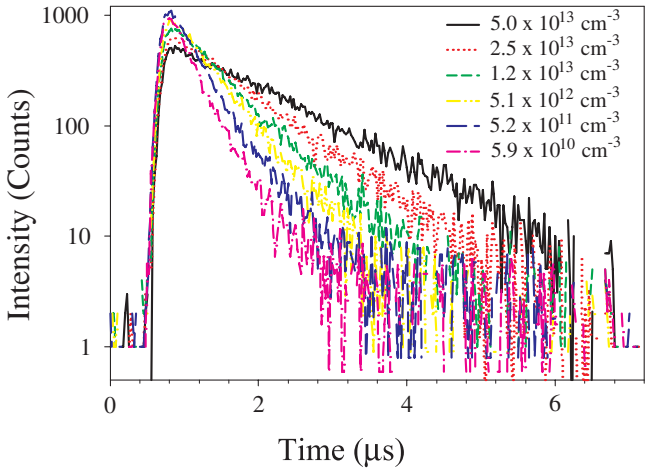

FIG. 3: Time-dependence of the light scattered during the F = 1 → F' = 2 optical pumping process. From upper to lower, the curves correspond to decreasing atomic density; the values refer to the peak density at the center of the sample. The correspondence between the peak density, the transverse optical depth, or the sample dimensions can be found in Table 1.

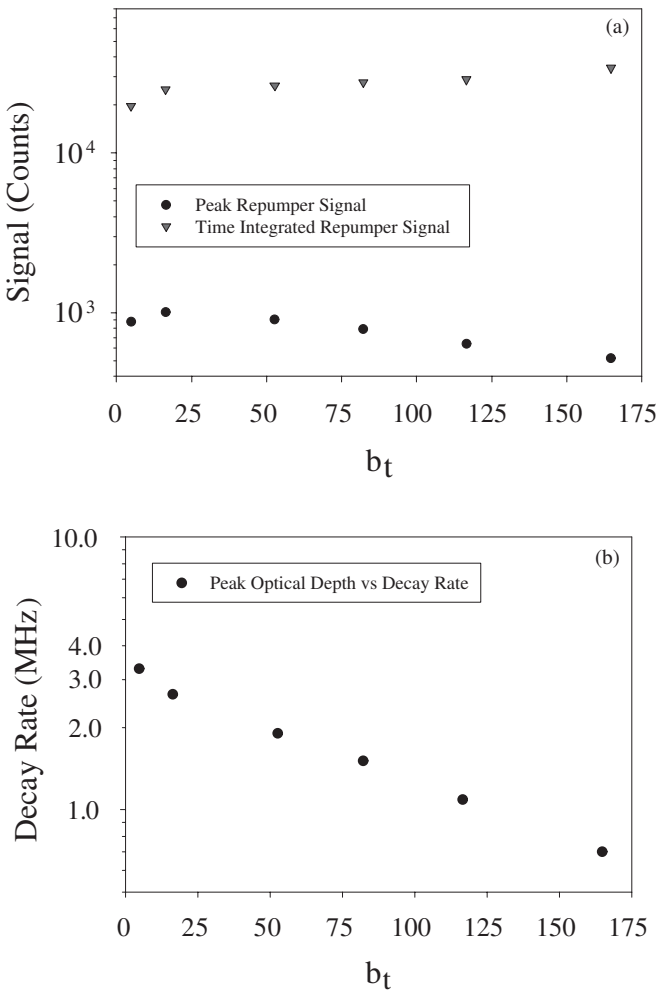

FIG. 4: Variations, with peak transverse optical depth, of measured quantities associated with the time and density dependence of the optical pumping transients, as extracted from the data of Figure 3. (a) Integrated and peak scattering signals, and (b) decay rate of the repumper transients.

by allowing for a selected period of free expansion of the sample prior to switching on the repumper laser and collecting the resulting scattered light signals. Further expansion of the sample during the data acquisition period is negligible. Several features of the data are apparent from Fig. 3. First, there is a small background signal of a few counts remaining even after the transient signals have decayed away. This behavior is more apparent in the lower density data, which has an associated faster decay rate than the higher density data. This signal is due to hot atom fluorescence excited by the intense repumper laser beams. Second, the decay of the signals is well approximated by a single exponential time decay, with the higher density data decaying at a much slower rate than the lower density measurements display. Finally, the total integrated intensity does not seem to vary much as the density is varied. These three features are summarized in Fig. 4. In this figure, the measured quantities are shown as a function of the peak transverse optical depth b_t. The connection between the various values of b_t and the peak atom density can be found in Table 1. In Fig. 4, we see that the peak scattered light intensity and the total (time-integrated) intensity does not vary strongly with optical depth. However, the exponential decay rate associated with the pumping process depends approximately exponentially itself on b_t. The time scale associated with the optical pumping process may be estimated by considering that the repumper laser beam is intense enough that it saturates the repumper transition. Then the time scale for the pumping process transferring an atom from the lower (F=1) to the upper (F = 2) hyperfine component is approximately $2\tau_o$, where $\tau_o \sim 26$ ns is the radiative lifetime of the excited state. On the average, then the repumper beam penetrates into the sample a distance of one optical mean free path $l = \frac{1}{\rho\sigma}$ in this time. Here ρ is the average atom density and σ is the optical scattering cross section [56] For a sample of size r_o, an estimate of the pumping time is then $T \sim 2\tau_o \frac{r_o}{l}$. This simple formula provides estimates in fair agreement with the results of Fig. 4(b).

Finally, we point out that in spite of the apparently simple phenomenology of the optical pumping dynamics, the physical process is in reality quite complex. For example, the atom sample is initially in the lower energy F = 1 hyperfine level, and after the process is terminated, is nearly completely pumped into the F = 2 level. At the same time, the atom sample is initially very optically deep to the repumper laser and optically thin to the F = 2

$\rightarrow$ F$'$ = 2 inelastic Raman decay. These roles are reversed but in a spatially inhomogeneous way as the pumping dynamics take place. Beyond this, multiply scattered light on both main transitions should participate significantly in the entire dynamics (this is ignored in the estimate of the pumping time above). Finally, the entire process is made yet more complex by the inelastic components in the scattered light, these being generated by the intense repumper laser. As this process is not the main focus of the present work, we defer theoretical modelling and more comprehensive experiments to a later study.

B. Combined Hyperfine Optical Pumping and Light Scattering on the $F = 2 \rightarrow F' = 3$ Transition

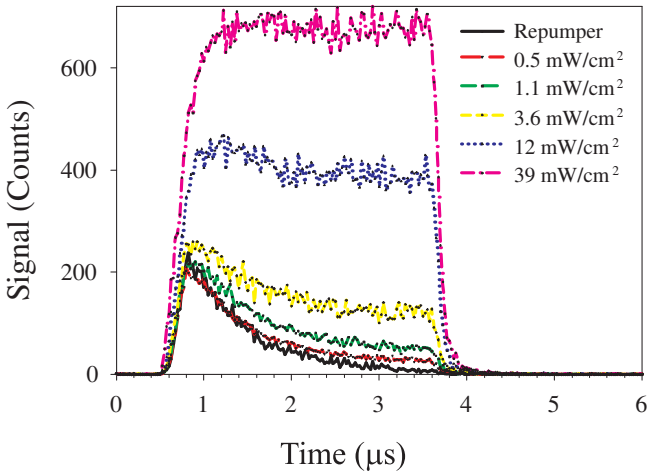

FIG. 5: Probe intensity dependence of the combined transients due to hyperfine optical pumping on the transition and light scattering on the nearly-closed F = 2 $\rightarrow$ F' = 3 transition.

We now consider measurements made of the time evolution of the light scattered from the sample when the repumping laser and a second probe laser beam are applied simultaneously to the sample. One main goal of these measurements is to find the approximate intensity range suitable for optical probing on the $F = 2 \rightarrow F' = 3$ transition, and to discover if there is significant trapping of probe light within the sample through the combined action of the repumper and probe excitations. For these measurements, the probe laser is tuned resonantly to the nearly-closed $F = 2 \rightarrow F' = 3$ hyperfine transition associated with the D2 component of the 5s - 5p multiplet. Results from these experiments are shown in Fig. 5, where the different curves correspond to different probe laser intensities. The repumper intensity is fixed, and at the same level as the results shown in Fig. 3. We see from Fig. 5 that the time evolution of the signals depends strongly on the probe laser intensity. For lower intensities, the time evolution is similar to that of the repumper laser alone, while for greater probe intensities, the signals more rapidly reach a nearly steady state level. The results may be qualitatively understood by considering that the atomic sample is initially optically very deep on the repumper transition, but becomes increasingly less so as a function of time. This behavior is evident from the data of Fig. 3. On the other hand, as the atoms are pumped to the F = 2 level, the optical depth associated with the $F = 2 \rightarrow F' = 3$ probe transition becomes increasingly large, the transverse optical depth becoming similar to that of Table 1 for later times. As the probe transition is nearly optically closed, we expect a steady scattering rate to be reached, and the data of Fig. 5 supports that expectation. The steady state level depends on the probe laser intensity, and the variations of this level are summarized in Fig. 6. There we see that the steady state level increases approximately linearly for lower intensities, but saturates at higher levels. However, the saturation parameter of unity for the probe transition is reached for a probe intensity of $I_s \sim 1.7 mW/cm^2$; the effective saturation evident in Fig. 6 occurs for much higher probe intensities than that. This may be physically understood through the fact that most of the atoms contributing to the signal are deep inside the atomic cloud, where the probe intensity is sharply decreased by scattering out of the coherent beam to be much smaller than the peak external value.

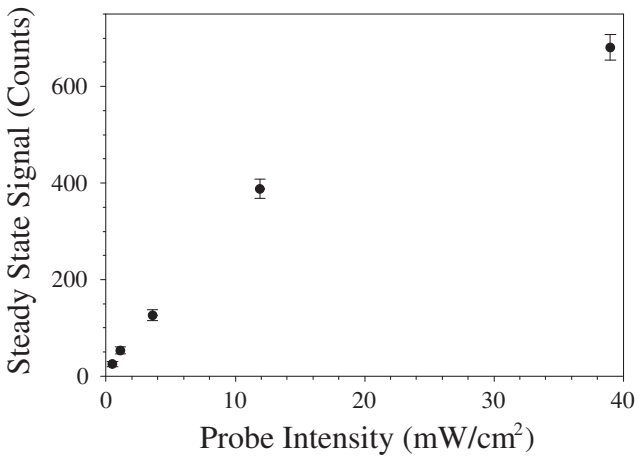

FIG. 6: Steady state signals as a function of F = 2 $\rightarrow$ F' = 3 probe laser intensity, as extracted from the data of Fig. 5.

C. Probe Light Scattering on the $F = 2 \rightarrow F' = 3$ Transition

1. *Density Dependence*

We now turn our attention to the main focus of this report, which is the situation where the hyperfine optical pumping process is completed prior to initiation of probe light scattering in the spectral vicinity of the $F = 2 \rightarrow F' = 3$ transition. In this case, the function of the hyperfine optical pumping is to transfer the atoms to the F = 2 ground level hyperfine component; when this process is complete, the peak resonance optical depth on the probe transition is about 165, as indicated in Table 1. We first consider the resonance response as a function of peak atom density under weak-field probe conditions of $\sim 630\ \mu W/cm^2$ (see Fig. 6). For these measurements, the atom sample is exposed to a nearly rectangular temporal pulse of 2 μs duration; this pulse has a 20 dB rise and fall time of about 100 ns. As shown in Fig. 7(a) and 7(b), the scattered light transients for all densities consist of a rather rapid increase to a steady level, followed by a several hundred nanosecond temporal decay after the probe laser beam is extinguished.

We further analyze these results by considering the integrated probe signal (as in Fig. 7) as a function of decreasing atomic density. However, instead of the atomic density, we parametrize the dependence in terms of the peak transverse optical depth b_t through the center of the ellipsoidal atomic sample. The optical depth is the natural parameter to describe many characteristics of light scattering and diffusion in dense scattering media, and the results described here are no exception. Note that there are nominally two optical depths required to describe our atomic sample [56]. These are the peak transverse optical depth b_t, as just mentioned, and the longitudinal optical depth b_l, which is typically more than 10 times larger than b_t. The variation of the integrated scattered light signals with b_t is shown in Fig. 8, where it is seen that the signals increase as the optical depth decreases. This behavior can be physically understood from the fact that for very large b_t, only the atoms near the sample surface contribute to the scattering signal. However, as the density, and correspondingly the optical depth, decreases, more of the atoms in the sample participate in the scattering, and the resulting signal increases.

To more quantitatively understand these results, we consider a simple model of light scattering from a spatially Gaussian atom distribution that is entirely illuminated by the probe beam. This model shows that the total (spatially integrated) scattered light intensity P_s should vary with optical depth b as [57]

$$P_s(b) = A\frac{1}{\eta b}\sum_{n=1}^{\infty}(-1)^{n+1}\frac{(\eta b)^n}{nn!} \qquad (3.1)$$

Here A is a constant proportional to $I_o N \sigma_o^2$, where I_o is the incident probe intensity, assumed to be uniform over the cross-section of the sample, N is the number of atoms in the sample, and σ_o is the resonance scattering cross section. b is the peak optical depth.

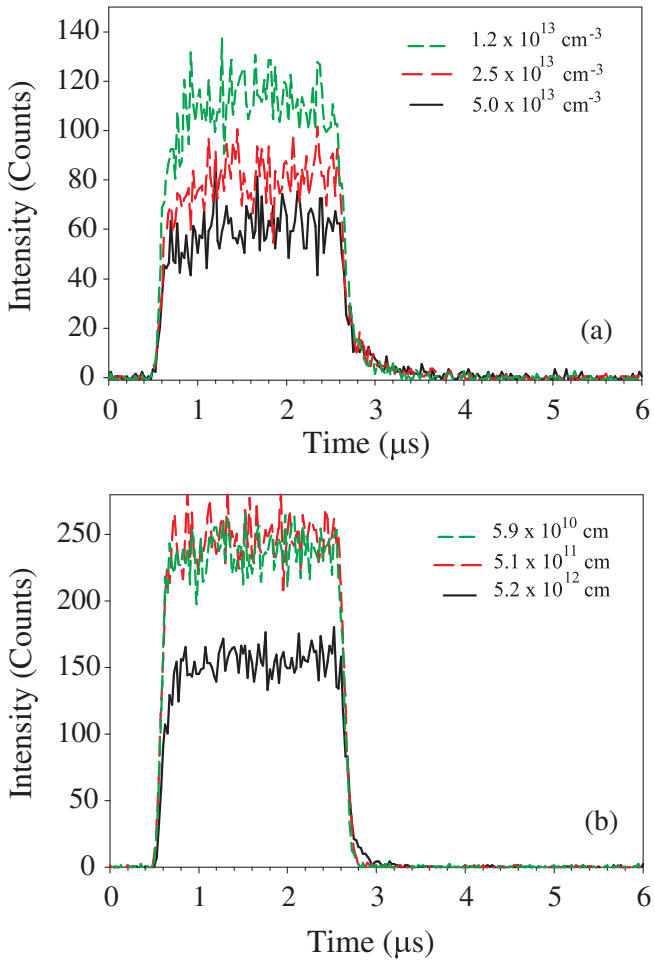

FIG. 7: Variations of the $F = 2 \rightarrow F' = 3$ resonant probe response with density and time. Note that the maximum intensity decreases with increasing density, at constant atom number. Note also the emergence of a long-time decay after the probe excitation is shut off. (a) Dependence for higher densities. (b) Dependence for lower intensities.

Here we make the assumptions that the optical depth corresponds to b_t (viz, Table 1) and that η is an empirical scaling parameter for the optical depth that is meant to measure the actual nonuniform spatial density distribution of the atomic sample and the limited penetration of the probe beam into the sample volume. This heuristic model describes the data of Fig. 8 well with values of A = 25(2) Kcounts, and η = 0.08(2). The small value of η is consistent with our expectation that the probe beam does not significantly penetrate the atomic vapor, even for the smallest transverse optical depth of about 5. The result of the two parameter fit of the expression for $P_s(b)$ to the density dependent data is shown as a solid curve

in Fig. 8.

Although this model gives a decent fit to the experimental data, it does not take into account the double Gaussian spatial distribution of atoms in the cloud or the angular distribution of the scattered intensity. More importantly, for the higher atomic densities corresponding to the larger optical depth parts of the data set, the scattering cross section departs from the free atom expression. As we describe in detail elsewhere [58], we have performed theoretical analysis and Monte Carlo simulations of the data in Fig. 8, and of data presented later in this paper. The fully quantal approach used has been described in detail previously [42], but has been generalized to account for the bi-Gaussian sample shape and for the particulars of the experimental excitation and detection geometries.

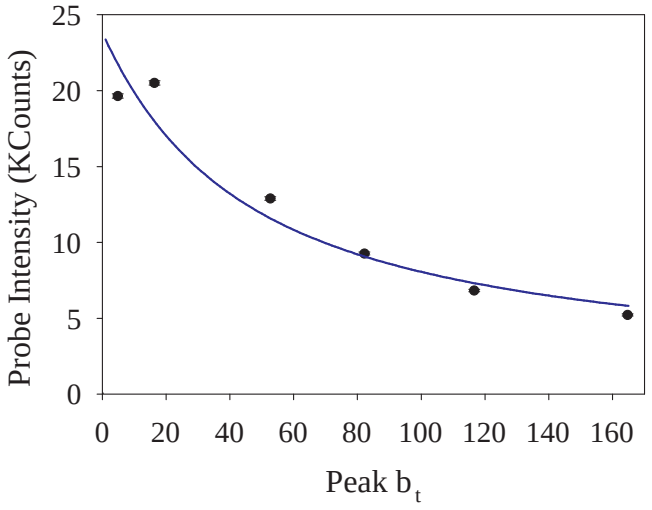

FIG. 8: Variations of the integrated $F = 2 \rightarrow F' = 3$ resonant probe response with peak transverse optical depth. Note that the maximum intensity decreases with increasing optical depth, at constant atom number.

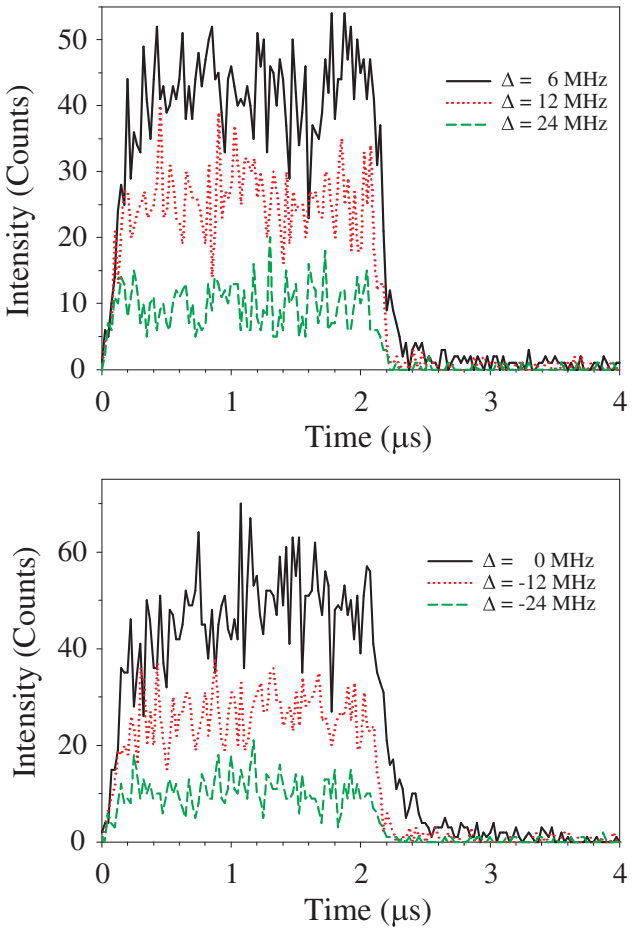

FIG. 9: Representative spectral variations of the transient light scattering response associated with the F = 2 → F' = 3 probe transition. Positive (higher frequency) detunings are shown in (a), while negative (lower frequency) detunings are shown in (b). These data are recorded under conditions of the peak transverse optical depth $b_t = 165$.

2. *Detuning Dependence*

We now turn to the detuning dependence of the light scattering signals. In these experiments we have measured the temporal response of the sample to a 2 μs probe pulse for detunings Δ in the range $\pm$ 24 MHz from the atomic $F = 2 \rightarrow F' = 3$ resonance. Positive values of Δ correspond to probe frequencies larger than the isolated atom resonance frequency. Representative measurements are given in Fig. 9 (a), (b), where we see that the response to the nearly rectangular probe pulse consists of a quite rapid increase in signal to a steady value (within the measurement statistics), followed by a clear decaying signal extending for nearly a μs after the probe beam is extinguished. These data are recorded under conditions of the peak transverse optical depth $b_t =$ 165. In analysis of this data, we first consider the temporally integrated signals as a function of detuning from atomic resonance; the resulting spectral variations are shown in Fig. 10. There we see that the response is approximately spectrally symmetric and has a full-width at half-maximum of about 24 MHz, corresponding to four times the natural width of the $F = 2 \rightarrow F' = 3$ transition under weak probe field conditions. Qualitatively, we expect broadening of the atomic response due to the large optical depth of the sample. We also note a small shift of the resonance response to frequencies lower than the single atom resonance. The frequency shift of about -0.8 MHz is of the right magnitude to correspond to the well-known Lorentz-Lorenz (local field) shift [59]. However, further measurements at higher density and with a spectrally narrower probe would be necessary to quantitatively examine that possibility.

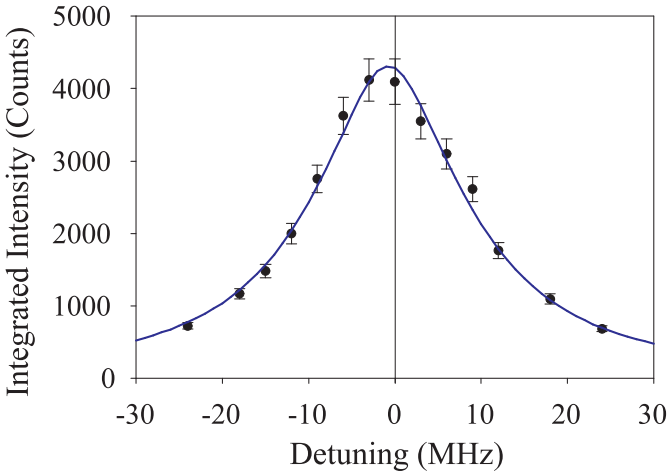

FIG. 10: Spectral variation of the temporally-integrated scattered light intensity on the F = 2 → F' = 3 transition. In this data the repumping process occurs first, and the near-resonance scattering signals are recorded after the repumping laser is turned off. These data are recorded under conditions of the peak transverse optical depth $b_t = 165$.

To analyze further this data, we return to the heuristic model we used in Section III.C.1, but taking into account the fact that the sample size remains fixed in these measurements, and that the optical depth varies with spectral detuning from atomic resonance. This model then gives

$$P_s(b) = A\sum_{n=1}^{\infty}(-1)^{n+1}\frac{(\eta b)^n}{nn!} \tag{3.2}$$

where

$$b(\Delta) = \frac{b_o}{1+(\frac{2(\Delta-\delta)}{\gamma'})^2} \tag{3.3}$$

Here A is proportional to $I_o r_o^2$, where I_o is the probe intensity, assumed uniform over the cloud dimensions and r_o is the Gaussian radius of the cloud. The quantity b_o is the peak optical depth, while δ accounts for the observed shift of the response profile. The spectral width γ' is assumed to be the 6 MHz width of the isolated atom response plus the spectral width of the probe laser. This part of the model assumes that the spectral response is the convolution of two Lorentzian line shapes. As before, we take b_o to be the peak on-resonance optical depth through the center of the cloud, and use η and δ as fitting parameters. The result of a fit with values of $\eta = 0.10(1)$ and $\delta = 0.8$ MHz is shown as a solid curve in Fig. 10. In this fit, the overall scattered intensity is scaled by the parameter A, which measures the fraction of the total intensity that is collected and measured in the experiment. The result is quite satisfactory, and the value of the empirical parameter η is also in satisfactory concordance with that obtained from fitting the density dependent data to the same model. The laser spectral width used in the fit is 3 MHz, consistent with the measured probe spectral profile.

Finally, we consider the longer time transients that appear once the probe laser beam is switched off. In the present case, when the probe is extinguished on a time scale fast compared to the emergence of light from the sample, the time scale is determined by diffusion of light from the interior of the sample to the surface, where it escapes and may be detected. We present in Fig. 11 an extended experimental run of longer than 10 hours. In Fig. 11(a) the entire response, which consists of the hyperfine pumping process and the probe excitation is displayed. In this case the probe pulse is 5 μs. In the figure, we see that there is a significant long time transient after the probe is shut off (vertical line). This long-time region is displayed with expanded horizontal and vertical scales in Fig. 11(b), where it is seen that the decay is characterized by multiple time scales, and that the decaying signals persist for longer than 2 μs. A fit of this data to a double exponential decay resulted in a high quality representation of the data with time constants of 100(10) ns and 500(50) ns. This fit is shown as the dashed line in Fig. 11(b).

To put the longer of these time scales in context, we again consider a spherically symmetric Gaussian ultracold atomic cloud. For that case, and for large optical depths, the longest lived diffusive mode has a decay time [21]

$$\tau = \frac{3b^2}{5.35\pi^2}\tau_o \tag{3.4}$$

where b is the peak optical depth and τ_o is the ~ 26 ns natural decay time of the excited level. If the atomic cloud in the present experiments were uniformly optically excited, the longest decay time should be about 40 μs, much longer than what is observed. We attribute this primarily to the relatively limited penetration of the probe beam into the atomic sample under the conditions of the present experiments. Using the same model considered before, if we replace b with $\eta b_t = 16.5$, this formula predicts a decay time of 420 ns, consistent with what we have measured.

We should point out that other factors, including suppression of the atomic cross section and the important role of atomic motion is also not negligible in these estimates. Motion of the atomic scatterers, for example, leads to a random walk in frequency space for the multiply scattered photons and, even for the atomic sample temperature of 65 μK, leads to a shortened lifetime for the longest lived diffusive mode.

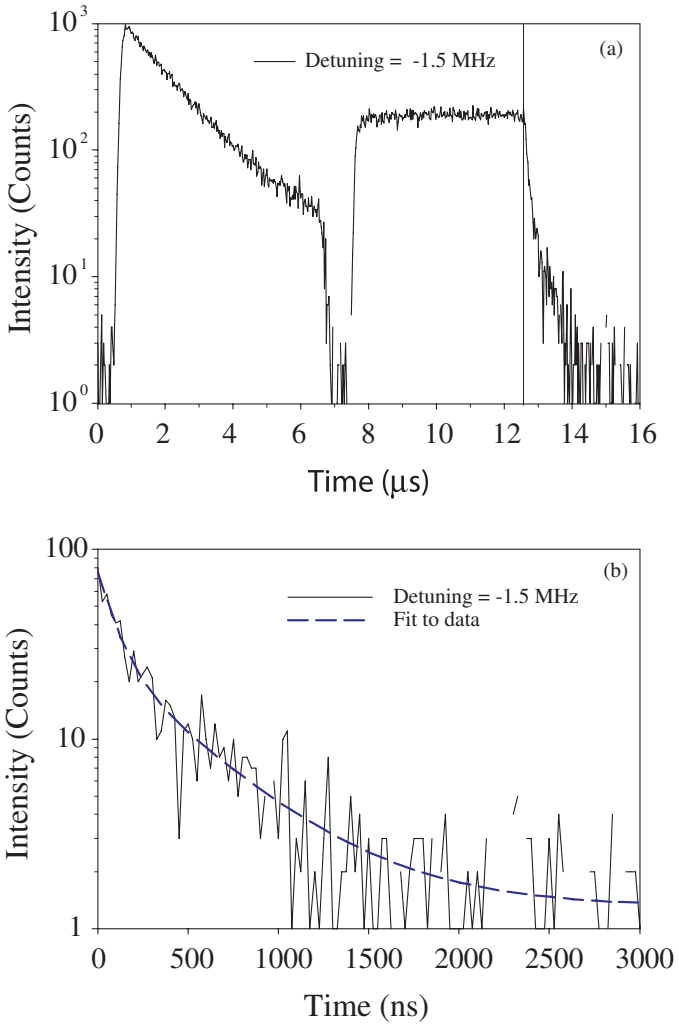

FIG. 11: Transient light scattering response associated with the F = 2 → F' = 3 transition. In this data the repumping process occurs first, and the near-resonance scattering signals are recorded after the repumping laser is turned off. Both the repumping signal and the overall transient response is shown in part (a). The vertical line represents where the probe beam is turned off. In part (b) we expand the scales to show the long-time transient after the probe beam is turned off.

IV. CONCLUSIONS

In this paper we have reported studies of near resonance light scattering from dense and ultracold atomic rubidium. The density is sufficiently large that the experimental conditions are close to satisfying the Ioffe-Regal criterion for localization on the optically closed $F = 2 \rightarrow F' = 3$ transition and on the optically open $F = 1 \rightarrow F' = 2$ hyperfine repumper transition. However, for the $F = 2 \rightarrow F' = 3$ transition, external the large optical depth of the sample does not permit injection of optical excitation to the highest density central portion of the sample. Observation of localization effects then do not seem possible using this scheme. For the $F = 1 \rightarrow F' = 2$ repumper transition, there is an open $F' = 2 \rightarrow F' = 2$ inelastic Raman decay channel which strongly inhibits multiple scattering, again making it challenging to observe localization effects. In spite of this, optical excitation on these transitions has revealed a variety of optical pumping and dynamical propagation effects which depend significantly on detuning from atomic resonance and on the optical depth of the atomic medium. For the case of a resonant probe beam incident on the cloud at maximum density, the light minimally penetrates into the medium, and the observed effects are due to scattering from atoms within a few optical mean free paths of the sample surface. This observation is supported by the relatively short diffusive lifetime of a few hundred ns for light emerging from the sample after the probe beam is turned off. Finally, to insure that light emerges from the sample via the longest lived mode will require alternative experimental schemes whereby photonic excitation may be injected directly into the highest density portions of the sample.

V. ACKNOWLEDGMENTS

We appreciate financial support of the National Science Foundation (Grant No. NSF-PHY-0654226), the Russian Foundation for Basic Research (Grant No. RFBR-08-02-91355), and INTAS (Project No. 7904).

[1] H.J. Metcalf and P. van der Straten, *Laser Cooling and Trapping*, Springer, New York, 1999.
[2] R. Grimm, M. Weidemuller, and Y. Ovchinnokov, Adv. Atom., Mol., and Opt. Phys. 42, 95 (2000).
[3] C.J. Pethick and H. Smith, *Bose-Einstein Condensation in Dilute Gases*, Cambridge University Press, Cambridge, UK, 2002.
[4] S. Giorgini, L.P. Pitaevskii, and S. Stringari, Rev. Mod. Phys. 80, 1215 (2008).
[5] Dirk Bouwmeester, Artur Ekert, and Anton Zeilinger, *The Physics of Quantum Information*, Springer-Verlag, Berlin, Germany, 2001.
[6] M.D. Lukin, Rev. Mod. Phys. 75, 457 (2003).
[7] P.W. Milonni, *Fast Light, Slow Light, and Left-handed Light*, Taylor and Francis, New York, 2005.
[8] M. Fleishhauer, A. Imamoglu, and J.P. Marangos, Rev. Mod. Phys. 77, 633 (2005).
[9] Lene Vestergaard Hau, Nature Photonics 2, 451 (2008).
[10] D.A. Braje, V. Balic, G.Y. Yin, and S.E. Harris, Phys. Rev. A 68, 041801 (2003).
[11] S. Ospelkaus, A. Peer, K.-K. Ni, J. J. Zirbel, B. Neyenhuis, S. Kotochigova, P. S. Julienne, J. Ye, and D. S. Jin, Nature Phys. 4, 622 (2008).
[12] G. K. Campbell, A. D. Ludlow, S. Blatt, J. W. Thomsen, M. J. Martin, M. H. de Miranda, T. Zelevinsky, M. M. Boyd, J. Ye, S. A. Diddams, T. P. Heavner, T. E. Parker,

and S. R. Jefferts, Metrologia 45, 539 (2008).
[13] Jun Ye, S. Blatt, M. M. Boyd, S. M. Foreman, E. R. Hudson, Tetsuya Ido, B. Lev, A. D. Ludlow, B. C. Sawyer, B. Stuhl, T. Zelinsky, Int. J. Modern Phys. D 16, 2481 (2007).
[14] Steven Rolston, Physics 1, 2 (2008).
[15] Thomas C. Killian, Science 316, 705 (2007).
[16] The entire issue, New J. Phys. 11 (2009), focuses on recent advances and opportunities in ultracold molecular physics. See particularly, Lincoln D. Carr and Jun Ye, New J. Phys. 11, 055009 (2009).
[17] Matthias Weidemüller and Claus Zimmermann, *Interactions in Ultracold Gases*, Wiley-VCH, Germany, 2003.
[18] M. Fleischhauer and M. D. Lukin, Phys. Rev. A 65, 022314 (2002).
[19] Y. O. Dudin, S. D. Jenkins, R. Zhao, D. N. Matsukevich, A. Kuzmich, and T. A. B. Kennedy, Phys. Rev. Lett. 103, 020505 (2009).
[20] Mark D. Havey, Contemporary Physics 50, 587 (2009).
[21] G.Labeyrie, Mod. Phys. Lett. B 22, 73 (2008).
[22] E. Akkermans and G. Montambaux, *Mesoscopic Physics of Electrons and Photons*, Cambridge University Press, Cambridge, 2007.
[23] D.V. Kupriyanov, I.M. Sokolov, C.I. Sukenik, and M.D. Havey, Laser Phys. Lett. 3, 223 (2006).
[24] Mark D. Havey and Dmitriy V. Kupriyanov, Phys. Scr. 72, C30 (2005).
[25] R. Kaiser and M.D. Havey, Optics and Photonics News 16, 38 (2005).
[26] C.A. Müller, T. Jonckheere, C. Miniatura, and D. Delande, Phys. Rev. A 64, 053804 (2001).
[27] A.F. Ioffe and A.R. Regel, Progr. Semicond. 4, 237 (1960).
[28] Y. Kuga and J. Ishimaru, J. Opt. Soc. Am. A 1, 831 (1984).
[29] P.E. Wolf and G. Maret, Phys. Rev. Lett. 55, 2696 (1985).
[30] G. Labeyrie, F. de Tomasi, J.-C. Bernard, C.A. Müller, C.A. Miniatura, and R. Kaiser, Phys. Rev. Lett. 83, 5266 (1999).
[31] B. R. Mollow, Phys. Rev. 188, 1969 (1969).
[32] G. Labeyrie, C.A. Müller, D.S. Wiersma, Ch. Miniatura, and R. Kaiser, J. Opt. B: Quantum Semiclass. Opt. 2, 672 (2000).
[33] Y. Bidel, B. Klappauf, J.C. Bernard, D. Delande, G. Labeyrie, C. Miniatura, D. Wilkowski, R. Kaiser, Phys. Rev. Lett. 88, 203902 (2002).
[34] G.Labeyrie, D. Delande, R.Kaiser, C. Miniatura, Phys. Rev. Lett. 97, 013004 (2006).
[35] G. Labeyrie, C. Miniatura, C. A. Müller, O. Sigwarth, D. Delande, R. Kaiser, Phys. Rev. Lett. 89, 163901 (2002).
[36] T. Chanelière, D. Wilkowski, Y. Bidel, R. Kaiser, and Ch Miniatura, Phys. Rev. E 70, 036602 (2004).
[37] D.V. Kupriyanov, I.M. Sokolov, and M.D. Havey, Optics Comm. 243, 165 (2004).
[38] P. Kulatunga, C.I. Sukenik, S. Balik, M.D. Havey, D.V. Kupriyanov, and I.M. Sokolov, Phys. Rev. A 68, 033816 (2003).
[39] D.V. Kupriyanov, I.M. Sokolov, N.V. Larionov, P. Kulatunga, C.I. Sukenik, S. Balik, and M.D. Havey, Phys. Rev. A 69, 033801 (2004).
[40] S. Balik, P. Kulatunga, C.I. Sukenik, M.D. Havey, D.V. Kupriyanov, and I.M. Sokolov, J. Mod. Optics 52, 2269 (2005).
[41] C. Cohen-Tannoudji, J. Dupont-Roc, G. Grynberg *Atom-Photon Interactions. Basic Processes and Applications* John Wiley & Sons,Inc., 1992.
[42] I.M. Sokolov, M.D. Kupriyanova, D.V. Kupriyanov, and M.D. Havey, Phys. Rev. A 79, 053405 (2009).
[43] E. Akkermans, A. Gero, and R. Kaiser, Phys. Rev. Lett. 101, 103602 (2008).
[44] P. W. Anderson, Phys. Rev. 109, 1492 (1958).
[45] D.S. Wiersma, P. Bartolini, Ad Lagendijk, and R. Righini, Nature 390, 671 (1997).
[46] A.A. Chabanov, M. Stoytchev, and A.Z. Genack,Nature 404, 850 (2000).
[47] M. Storzer, P. Gross, C.M. Aegerter, and G. Maret, Phys. Rev. Lett. 96, 063904 (2006).
[48] C.M. Aegerter and G. Maret, *Coherent backscattering and Anderson localization of light*, in Progress in Optics 52, 1 (2009).
[49] Hui Cao, *Lasing in Disordered Media*, in Progress in Optics 45, (2003).
[50] D.S. Wiersma, Nature Phys. 4, 359 (2008).
[51] C. Conti and A. Fratalocchi, Nature Phys. 4, 794 (2008).
[52] L. Froufe-Pèrez, W. Guerin, R. Carminati and R. Kaiser Phys. Rev. Lett.102, 173903 (2009).
[53] W. Guerin, N. Mercadier, D. Brivio and R. Kaiser, Optics Exp. 17, 14 (2009).
[54] Joel Keizer, *Statistical Thermodynamics of Nonequlibrium Processes*, Springer-Verlag, New York, 1987; Bruce J. Berne and Robert Pecora, *Dynamic Light Scattering*, John Wiley and Sons, New York, 1976.
[55] S. Balik, A.L. Win, and M.D. Havey, Phys. Rev. A 80, 023404 (2009).
[56] For an ellipsoidal Gaussian atom distribution of sizes r_o and z_o and peak density n_o, $n(r) = n_o e^{-r^2/2r_o^2 - z^2/2z_o^2}$. The total number of atoms is $N = (2\pi)^{3/2} n_o r_o^2 z_o$ and the peak transverse (longitudinal) optical depth is $b_t = \sqrt{2\pi} n_o \sigma_o r_o$ ($b_l = \sqrt{2\pi} n_o \sigma_o z_o$). σ_o is the weak field resonance light scattering cross section. The peak total cross-section is given by $\frac{2F'+1}{2F+1}\frac{\lambda^2}{2\pi}$.
[57] S. Balik, M.D. Havey, I.M. Sokolov, and D.V. Kupriyanov, Phys. Rev. A 79, 033418 (2009).
[58] I.M. Sokolov, D.V. Kupriyanov and M.D. Havey, to be published.
[59] J.J. Maki, M. S. Malcuit, J.E. Sipe, and R.W. Boyd, Phys. Rev. Lett. 67, 972 (1991).